Phase-Contrast Tomographic Imaging Using an X-ray Interferometer

Atsushi Momose,[a]* Tohoru Takeda,[b] Yuji Itai,[b] Akio Yoneyama[c] and Keiichi Hirano[d]

[a]*Advanced Research Laboratory, Hitachi Ltd, Hatoyama, Saitama 350-03, Japan,* [b]*Institute of Clinical Medicine, University of Tsukuba, Tsukuba, Ibaraki 305, Japan,* [c]*Central Research Laboratory, Hitachi Ltd, Kokubunji, Tokyo 182, Japan, and* [d]*Institute of Materials Structure Science, High Energy Accelerator Research Organization, Tsukuba, Ibaraki 305, Japan.* E-mail: momose@harl.hitachi.co.jp

Apparatus for phase-contrast X-ray computed tomography using a monolithic X-ray interferometer is presented with some observational results for human breast tissues. Structures characteristic of the tissues were revealed in the phase-contrast tomograms. The procedure of image analysis consists of phase retrieval from X-ray interference patterns and tomographic image reconstruction from the retrieved phase shift. Next, feasibility of phase-contrast imaging using a two-crystal X-ray interferometer was studied aiming at *in vivo* observation in the future. In a preliminary study, the two-crystal X-ray interferometer was capable of generating fringes of 70% visibility using synchrotron X-rays.

Keywords: phase contrast; tomography; X-ray interferometers; phase retrieval; cancer.

1. Introduction

When X-rays travel through an object, both amplitude and phase of the X-ray wave are modified by the object. In conventional X-ray transmission imaging, contrast is generated from the change in the amplitude. However, especially in the hard X-ray energy region, the amplitude contrast (absorption contrast) is insufficient for investigating materials consisting of light elements which do not absorb X-rays as much. Recently, phase-contrast X-ray imaging has been studied actively. Because the phase-shift cross section is much larger than the absorption cross section, high sensitivity to organic structures is expected with a reasonable X-ray dose.

To obtain contrast related to the X-ray phase shift, several techniques are studied. In the soft X-ray energy region, holographic imaging (see, for example, Aoki & Kikuta, 1974; Jacobsen *et al.*, 1990; McNulty *et al.*, 1992; Lindaas *et al.*, 1996; Shinohara *et al.*, 1996) and Zernike's phase-contrast microscopy (Schmahl *et al.*, 1994) have been reported. In the hard X-ray energy region, an interferometric method (Bonse & Hart, 1965*a*; Ando & Hosoya, 1972; Momose & Fukuda, 1995; Takeda *et al.*, 1995) using a crystal X-ray interferometer (Bonse & Hart, 1965*b*), a Schlieren-like method using crystal diffraction (Forster *et al.*, 1980; Somenkov *et al.*, 1991; Davis *et al.*, 1995*a,b*; Ingal & Beliaevskaya, 1995), a holography-like method (Snigirev *et al.*, 1995*a,b*; Cloetens *et al.*, 1996; Raven *et al.*, 1996), and others (Nugent *et al.*, 1996; Wilkins *et al.*, 1996; Snigirev *et al.*, 1997) have been studied.

The purpose of our research is three-dimensional observation of biological soft tissues with hard X-ray phase contrast. We started from the interferometric method which is sufficiently sensitive to the phase shift caused by biological soft tissues. To achieve three-dimensional observation, the technique of X-ray computed tomography is useful. However, interference patterns cannot be processed under a tomographic configuration as they are. According to the principle of X-ray computed tomography, the input data to the reconstruction algorithm should be a projection of a quantity f that conveys structural information inside a sample. Then, one can obtain a tomogram which maps the value f. In the scheme of absorption-contrast tomography, the logarithm of the X-ray transmittance is used as input data. Because it is a projection of the linear absorption coefficient μ, the spatial distribution of μ can be revealed in a tomogram. We can find a similar relation in the phase shift process. Because the phase shift corresponds to the projection of the refractive index, the distribution of the refractive index can be reconstructed by processing the phase shift. We define this procedure as phase-contrast X-ray computed tomography. In this case, we have to measure the spatial distribution of the phase shift (phase-mapping image). Therefore, a conversion method from X-ray interference patterns to the phase-mapping images is necessary.
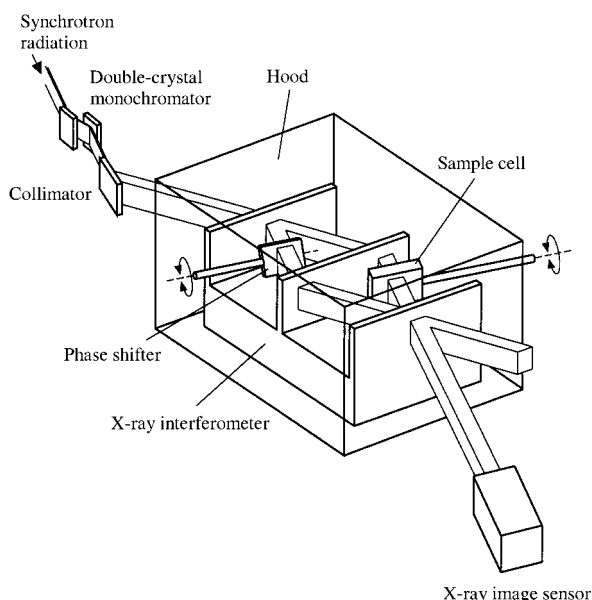
A breakthrough was obtained by introducing one of the subfringe analysis methods, which were originally developed in visible light interferometry. Momose (1995)

adopted the fringe scanning method (Bruning *et al.*, 1974), and realised phase-contrast X-ray computed tomography for the first time. It was shown that the sensitivity was substantial enough to depict structures inside soft tissues without staining (Momose *et al.*, 1995, 1996*a,b*; Bonse & Busch, 1996; Momose, Takeda, Itai & Hirano, 1997; Beckmann *et al.*, 1997). In this paper, we report our recent apparatus of phase-contrast X-ray computed tomography with some observational examples of human breast tissues.

Hard X-rays are useful in investigating structures inside thick samples non-destructively. As a next step, therefore, we aim at applications of this technique to *in vivo* observation. Momose, Takeda & Itai (1997) have so far estimated optimal X-ray energy for minimizing the dose as a function of sample size. An important instrumental subject is to widen the size of the view field. This means that a large X-ray interferometer should be developed. Because the interferometer currently used for phase-contrast X-ray computed tomography is monolithically cut out of an ingot of silicon crystal, the size of the interferometer is limited by the size of the ingot. Instead, we checked the feasibility of phase-contrast imaging using the two-crystal X-ray interferometer reported by Becker & Bonse (1974). In a preliminary study, the two-crystal interferometer was capable of generating interference fringes of 70% visibility at a synchrotron radiation facility (Momose, Yoneyama & Hirano, 1997). The details of the experiment are also reported in this paper.

2. Procedure of image analysis

*Phase-contrast imaging* is used to imply that X-ray phase information is related to the generation of contrast. The physical meaning of the obtained contrast is different depending on the methods. In the case of the interferometric method, one can observe fringes which appear every 2π phase shift. Using the holography-like method, fringes caused by Fresnel diffraction are seen. In the case of the Schlieren-like method, a part of a specific phase gradient is emphasized.

In every case, observable images are different from the phase-mapping image. Therefore, to achieve phase-contrast X-ray computed tomography, a technique is needed to obtain the phase-mapping images from phase-contrast images. Absorption contrast superposed in the phase-contrast images should also be removed in this process. We used the interferometric method to measure the phase-mapping images as below.

In visible light interferometry, techniques for the measurement of the phase shift have been developed. We have introduced one of the techniques (fringe scanning method) to X-ray interferometry. With the fringe scanning method, the phase-mapping image can be calculated from several interference patterns which are obtained by changing the phase difference step by step between the object beam and the reference beam. The phase difference is created, for instance, by placing a tunable phase shifter in the beam path. When M interference patterns are obtained by changing the phase difference in $2\pi/M$ steps, the phase-mapping image Φ is calculated as

$$\Phi = \mathrm{Arg}\left[\sum_{k=1}^{M} I_k \exp(-2\pi i k/M)\right], \qquad (1)$$

where I_k is the interference pattern obtained when the phase difference is $2\pi k/M$. Arg[. . .] indicates the extraction of the argument. Φ, calculated using (1), is wrapped within the range from $-\pi$ to π. Therefore, to obtain a real phase shift, the phase jump of 2π must be compensated. The phase-unwrapping process is easy when the phase gradient is not so steep compared with the resolution of an image sensor. With these procedures, the

Figure 1
Experimental set-up of phase-contrast X-ray computed tomography.
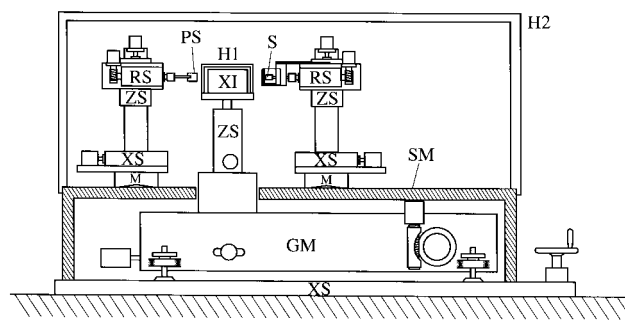
Figure 2
A schematic view of the apparatus of phase-contrast X-ray computed tomography. XI: X-ray interferometer; GM: goniometer for the interferometer; XS: horizontal linear stage; ZS: vertical linear stage; RS: rotation stage; SM: base; H1 and H2: hoods; S: sample; PS: phase shifter.

influence of absorption is removed and a pure phase-mapping image can be obtained.

Usually the crystal X-ray interferometer has a built-in Moiré pattern caused by deformation of the inter-ferometer. In the measurement of the phase-mapping images, the Moiré pattern is not crucial because the Moiré pattern can be processed as a phase background. There-fore, the real phase shift caused by a sample can be obtained by subtracting the phase background, which can be measured in advance without the sample.

Currently, phase-mapping images are obtained only by using the interferometric method in combination with the fringe scanning method. If phase-mapping images are obtained with other phase-contrast methods, phase-contrast tomography can be carried out in the same manner.

3. Experiments

3.1. Apparatus

The experiments were performed at the station BL-14B of the Photon Factory, Tsukuba, Japan, where hard X-rays from a vertical wiggler were available. A beam through a Si(111) double-crystal monochromator was introduced into an experimental hutch. As shown in Fig. 1, the section of the beam was expanded with an asymmetrically cut Si(220) crystal (collimator). We used a typical triple Laue-case X-ray interferometer with Si(220) reflection. The thickness of the crystal wafers was 1 mm, and the gap between them was 34 mm. The wafers functioned as X-ray half mirrors for X-rays which satisfied the diffraction condition in a Laue geometry. Consequently, Mach–Zehnder-type optical beam paths were created. Putting a sample in one of the paths of the beams, an interference pattern corresponding to the phase shift caused by the sample was detected in the outgoing beams from the interferometer. The sample was rotated in a cell filled with water. With this cell, a wet sample was observable, and interference fringes caused by the outline structure of the

sample were moderately reduced (see Momose, 1995). A 0.5 mm-thick plastic plate was placed in the other beam path to obtain a phase-mapping image with the fringe scanning method. The relative phase difference between the two interfering beams was tuned by rotating the plate. X-ray interference patterns were obtained with the X-ray sensing pickup tube (Suzuki *et al.*, 1989) operated at a pixel size of 12×12 µm. To stabilize the interferometer, it was covered with a hood. Otherwise, the phase relation between the two interfering beams would no longer be stable because a temperature gradient caused by air flow would deform the interferometer. In such a case, the determination accuracy of the phase shift decreased. Occasionally, the interference pattern smeared out.

Fig. 2 shows a schematic view of the apparatus for phase-contrast X-ray computed tomography. The X-ray interferometer was placed on a table of a goniometer whose rotation accuracy was $0.01''$. Stages of the sample and the phase shifter were fixed on a base. The base was isolated from the goniometer for the interferometer to prevent vibration caused by the rotation of the sample and the phase shifter from disturbing interference. The designs of the stages for the sample and phase shifter were almost the same. Each stage consisted of horizontal and vertical linear stages and a rotation stage of the horizontal axis. The displacement of the sample rotation axis was designed within 2 µm over $360°$ rotation. All translations and rota-tions were controlled by pulse motors. The interferometer was covered with a hood to reduce the phase fluctuation, as mentioned above. On all sides of the hood, polymer sheets were attached. Because holes in the polymer sheets were made for the insertion of the sample and phase shifter, the effect of the hood was insufficient. Therefore, a larger hood was also used to cover the whole space on the base. The walls of the hood were made of acrylic resin. X-ray beams passed through holes made in the walls, where polymer films were attached. By using this apparatus, the X-ray interferometer was sufficiently stable during the measurement.
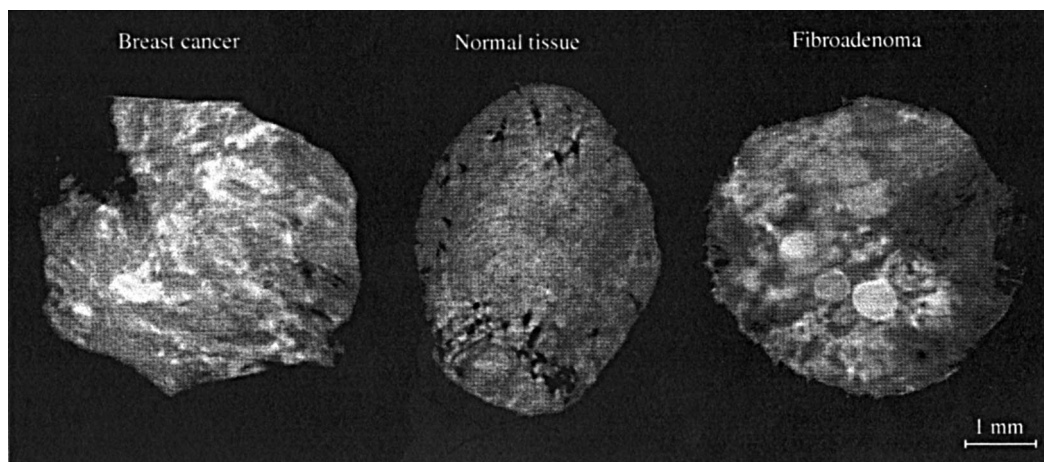
Figure 3
Phase-contrast tomograms of human breast tissues.

3.2. *Phase-contrast tomograms of human breast tissues*

We have carried out observations of some human tissues extirpated and fixed in formalin to obtain knowledge of the structures detectable with hard X-ray phase contrast. In this paper, we present observational results of human breast tissues. Fig. 3 shows phase-contrast tomograms of a normal tissue, breast cancer, and fibroadenoma (benign tumor). The tomograms were obtained with 17.7 keV X-rays. The number of the steps of the fringe scan was ten, and the sample was rotated in 0.9° steps. For the reconstruction of the tomograms, a normal convolution method was used. The pixel size of the tomograms was 12×12 μm, and the thickness of the section was also 12 μm. Although the samples did not contain any calcification, clear structures were depicted in the tomograms. Detailed histological analyses of the tomograms are in progress.
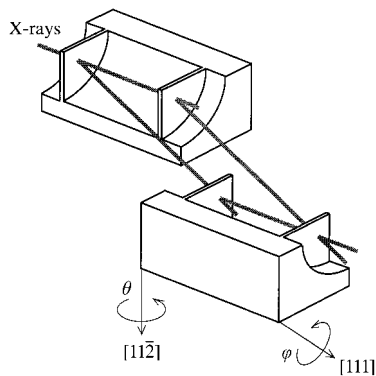
3.3. *Two-crystal X-ray interferometer*

As a next step, we aim at *in vivo* observation using the phase-contrast technique. For this purpose, a view area more than 2 cm square is desirable. As mentioned, the maximum size of the monolithic interferometer is limited by the size of a silicon ingot. A possible solution for the requirement is to develop an interferometer consisting of two independent crystal blocks. By aligning the blocks with a proper distance, a large view area can be obtained.

However, precise tuning stages should be constructed for the alignment of the two blocks. Of course, one has to be prepared for the influence of vibration and temperature drift. The two-crystal interferometer shown in Fig. 4 is advantageous for our purpose. With this constitution, the influence of the parallel displacement between the two blocks is completely cancelled. Required tuning axes are θ and φ, shown in Fig. 4. When the φ axis is detuned, a pattern similar to the rotational Moiré fringes appears. The origin of the fringes has been explained by Becker & Bonse (1974), and the spacing Λ of the Moiré fringes is

$$\Lambda = \lambda L / 2x \Delta\varphi \sin\theta_B, \qquad (2)$$

where λ, L, x and θ_B are the X-ray wavelength, the distance from the source to the image sensor, the length of

the beam path between the wafers on each block, and the Bragg diffraction angle, respectively. When a synchrotron source is used, L is much larger than x. Therefore, the influence of $\Delta\varphi$ is not serious. We can use a normal tilt stage to tune φ. Furthermore, it should be noted that we do not need to remove the Moiré fringes completely. When the fringe scanning method is used, the Moiré fringes can be processed as a phase background. It is required that the φ axis is tuned within the range where the fringe spacing of the Moiré fringes is sufficiently larger than the spatial resolution of the image sensor. Misalignment of about 0.1 mrad is permissible.

Therefore, we can concentrate only on tuning the θ axis to generate interference. The rotation around the θ axis is equivalent to a lever motion which causes a displacement Δs of a wafer against the other wafer on the block in the direction normal to the Bragg plane. In this case, a nominal phase difference of 2π is generated when Δs corresponds to the Bragg plane spacing. Becker & Bonse (1974) have shown that the phase difference $\Delta\Phi$ is

$$\Delta\Phi = 2\pi\Delta s / d, \qquad (3)$$

where d is the Bragg plane spacing. Thus, θ should be kept stable so that Δs is sufficiently smaller than the Bragg plane spacing. Otherwise, the interference pattern smears out. However, a slow drift of θ compared with the time of the fringe scan is permissible, because an interference pattern is observable in a wider angular range.

Phase-contrast imaging with the two-crystal interferometer has not been tried using synchrotron X-rays, as far as we know. Therefore, we have attempted to demonstrate that the two-crystal X-ray interferometer functions in the environment of a synchrotron facility. We fabricated a two-crystal X-ray interferometer consisting of small blocks [but larger than those of Becker & Bonse (1974)]. The thickness of the wafers was 1 mm and the gap between them was 34.5 mm. To tune the θ axis, a stage of a monolithic flexure hinge structure, shown in Fig. 5, was fabricated. Half of the stage was moved by a piezoelectric device around a hinge A. The stage was also linked at B to

Figure 4
Two-crystal X-ray interferometer.
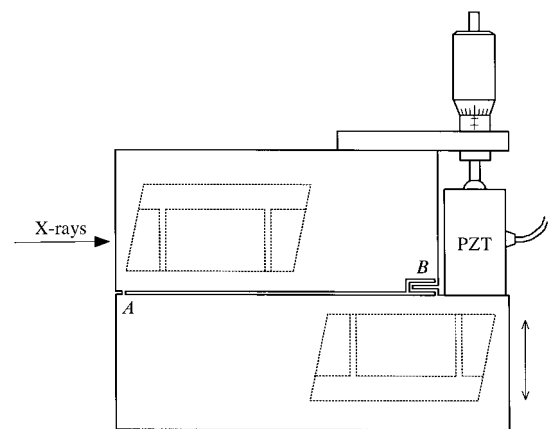
Figure 5
A stage for the alignment of the two-crystal X-ray interferometer.
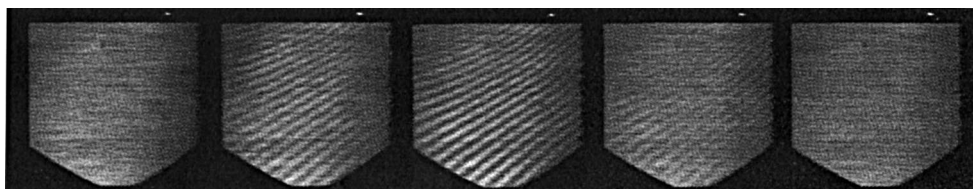
Figure 6
Interference patterns generated by the two-crystal X-ray interferometer. Five interference patterns were obtained varying θ in 1 µrad steps. Fringes of 0.5 mm spacing were generated with 70% visibility.

make the stage rigid in the direction parallel to the rotation axis. The structure at *B* functioned as a spring. Two crystal blocks of the interferometer were placed on the stage as shown in Fig. 5 with dotted lines. A tilt stage for tuning the φ axis was placed between the stage and the crystal block (not shown). To reduce the influence of vibration, the experiment was carried out on a massive stage with pneumatic sustainment.

In the experiment, we used 13.5 keV X-rays with the (220) reflection at the same station as the tomographic experiments. The stage shown in Fig. 5 was put on a goniometer to tune the incident angle of X-rays to the first block of the two-crystal interferometer. After the Bragg diffraction condition was satisfied for the first block, the θ axis of the second block was tuned. Because the stroke was limited with the piezoelectric device, the two blocks were prealigned to be almost parallel using an autocollimator. The blocks were fabricated in an identical shape, and side facets of the blocks were used to set them in parallel. To find an interference pattern, the θ axis was scanned within the angular range of the Bragg diffraction of the second block.

Fig. 6 shows the interference patterns obtained varying θ in 1 µrad steps. The exposure time was 4 s to obtain each interference pattern. Fringes were visible within an angular range of about 4 µrad around the θ axis. In this experiment, no sample was placed in the beam paths. Therefore, the observed fringes (0.5 mm spacing) were caused by deformation of the interferometer, lattice strain of silicon crystal, and misalignment around the φ axis. However, the fringe visibility was 70% at the best position, which is sufficient for fringe analysis using the fringe scanning method.

4. Summary

Currently, soft structures, such as cancer, can be revealed only by the interferometric method among the phase-contrast imaging methods proposed using hard X-rays. Phase-contrast X-ray computed tomography has been developed based on the interferometric method in combination with the fringe scanning method. In this paper, our apparatus for phase-contrast X-ray computed tomography has been presented with observational results for human breast tissues. Structures characteristic of the tissues have been depicted. The structures revealed in the

phase-contrast tomograms hardly create contrast in a mammogram currently used to diagnose breast cancer.

Such quality of the phase-contrast tomograms motivated us to develop a two-crystal X-ray interferometer. By creating a wider observation field with the interferometer, we aim at *in vivo* observations. Apparatus for studying the feasibility of phase-contrast X-ray imaging using the two-crystal X-ray interferometer was presented. An interference pattern, whose visibility was sufficient for the fringe analysis, was generated at the Photon Factory. This result proves the possibility for *in vivo* phase-contrast imaging in the future.

References

Ando, M. & Hosoya, S. (1972). *Proceedings of the 6th International Conference on X-ray Optics Microanalysis*, edited by G. Shinoda, K. Kohra & T. Ichinokawa, pp. 63–68. University of Tokyo Press.

Aoki, S. & Kikuta, K. (1974). *Jpn. J. Appl. Phys.* **13**, 1385–1392.

Becker, P. & Bonse, U. (1974). *J. Appl. Cryst.* **7**, 593–598.

Beckmann, F., Bonse, U., Busch, F. & Günnewig, O. (1997). *J. Comput. Assist. Tomogr.* **21**, 539–553.

Bonse, U. & Busch, F. (1996). *Prog. Biophys. Mol. Biol.* **65**, 133–169.

Bonse, U. & Hart, M. (1965*a*). *Appl. Phys. Lett.* **7**, 99–101.

Bonse, U. & Hart, M. (1965*b*). *Appl. Phys. Lett.* **6**, 155–156.

Bruning, J. H., Herriott, D. R., Gallagher, J. E., Rosenfeld, D. P., White, A. D. & Brangaccio, D. J. (1974). *Appl. Opt.* **13**, 2693–2703.

Cloetens, P., Barratt, R., Baruchel, J., Guigay, J.-P. & Schlenker, M. (1996). *J. Phys. D*, **29**, 133–146.

Davis, T. J., Gao, D., Gureyev, T. E., Stevenson, A. W. & Wilkins, S. W. (1995*a*). *Nature (London)*, **373**, 595–598.

Davis, T. J., Gureyev, T. E., Gao, D., Stevenson, A. W. & Wilkins, S. W. (1995*b*). *Phys. Rev. Lett.* **74**, 3173–3176.

Forster, E., Goetz, K. & Zaumseil, P. (1980). *Krist. Tech.* **15**, 937–945.

Ingal, V. N. & Beliaevskaya, E. A. (1995). *J. Phys. D*, **28**, 2314–2317.

Jacobsen, C., Howells, M., Kirz, J. & Rothman, S. (1990). *J. Opt. Soc. Am.* A**7**, 1847–1861.

Lindaas, S., Howells, M., Jacobsen, C. & Kalinovsky, A. (1996). *J. Opt. Soc. Am.* A**13**, 1788–1800.

McNulty, I., Kirz, J., Jacobsen, C., Anderson, E. H., Howells, M. R. & Kern, D. P. (1992). *Science*, **256**, 1009–1012.

Momose, A. (1995). *Nucl. Instrum. Methods*, A**352**, 622–628.

Momose, A. & Fukuda, J. (1995). *Med. Phys.* **22**, 375–380.

Momose, A., Takeda, T. & Itai, Y. (1995). *Rev. Sci. Instrum.* **66**, 1434–1436.

Momose, A., Takeda, T. & Itai, Y. (1997). *Proc. SPIE*, **3149**, 120–129.

Momose, A., Takeda, T., Itai, Y. & Hirano, K. (1996*a*). *Proc. SPIE*, **2708**, 674–684.

Momose, A., Takeda, T., Itai, Y. & Hirano, K. (1996*b*). *Nature Med.* **2**, 473–475.

Momose, A., Takeda, T., Itai, Y. & Hirano, K. (1997). *X-ray Microscopy and Spectromicroscopy*, edited by J. Thieme, G. Schmahl, E. Umbach & D. Rudolph. Heidelberg: Springer-Verlag.

Momose, A., Yoneyama, A. & Hirano, K. (1997). *J. Synchrotron Rad.* **4**, 311–312.

Nugent, K. A., Gureyev, T. E., Cookson, D. F., Paganin, D. & Barnea, Z. (1996). *Phys. Rev. Lett.* **77**, 2961–2964.

Raven, C., Snigirev, A., Snigireva, I., Spanne, P., Souvorov, A. & Kohn, V. (1996). *Appl. Phys. Lett.* **69**, 1826–1828.

Schmahl, G., Gutmann, P., Schneider, G., Niemann, B., David, C., Wilhein, T., Thieme, J. & Rudolph, D. (1994). *X-ray Microscopy IV*, edited by V. V. Aristov & A. I. Erko, pp. 196–206. Bogorodskii Pechatnik, Chernogolovka, Russia.

Shinohara, K., Ito, A., Nakano, H., Kodama, I., Honda, T., Matsumura, T. & Kinoshita, K. (1996). *J. Synchrotron Rad.* **3**, 35–40.

Snigirev, A., Snigireva, I., Bosecke, P., Lequien, S. & Schelokov, I. (1997). *Opt. Commun.* **135**, 378–384.

Snigirev, A., Snigireva, I., Kohn, V., Kuznetsov, S. & Schelokov, I. (1995*a*). *Rev. Sci. Instrum.* **66**, 5486–5492.

Snigirev, A., Snigireva, I., Suvorov, A., Kocsis, M. & Kohn, V. (1995*b*). *ESRF Newsl.* **24**, 23–25.

Somenkov, V. A., Tkalich, A. K. & Shil'shtein, S. Sh. (1991). *Sov. Phys. Tech. Phys.* **36**, 1309–1311.

Suzuki, Y., Hayakawa, K., Usami, K., Hirano, T., Endoh, T. & Okamura, Y. (1989). *Rev. Sci. Instrum.* **60**, 2299–2302.

Takeda, T., Momose, A., Itai, Y., Wu, J. & Hirano, K. (1995). *Acad. Radiol.* **2**, 799–803.

Wilkins, S. W., Gureyev, T. E., Gao, D., Pogany, A. & Stevenson, A. W. (1996). *Nature (London)*, **384**, 335–338.